

Florida Institute of Technology

Scholarship Repository @ Florida Tech

Theses and Dissertations

5-2021

Scaling Laws for Fixed-Wing Single-Engine Electric Propulsion Systems

Fnu Hem Lata

Follow this and additional works at: <https://repository.fit.edu/etd>



Part of the [Aerospace Engineering Commons](#)

Scaling Laws for Fixed-Wing Single-Engine Electric Propulsion Systems

By

FNU HEM LATA

A thesis submitted to the College of Engineering and Science of
Florida Institute of Technology
in partial fulfillment of the requirements
for the degree of

Master of Science
in
Flight Test Engineering

Melbourne, Florida
May, 2021

We the undersigned committee hereby approve the attached thesis,
"Scaling Laws for Fixed-Wing Single-Engine Electric Propulsion Systems"
by
FNU Hem Lata

Brian Kish, Ph.D.
Associate Professor, Program Chair,
Flight Test Engineering &
Aerospace, Physics and Space Sciences
Major Advisor

Markus Wilde, Ph.D.
Associate Professor
Aerospace, Physics and Space Sciences
Committee Member

Isaac Silver, Ph.D.
Associate Professor
College of Aeronautics
Committee Member

David Fleming, Ph.D.
Associate Professor, Department Head
Aerospace Physics and Space Sciences
Committee Member

Abstract

Title: Scaling Laws for Fixed-Wing Single-Engine Electric Propulsion Systems

Author: FNU HEM LATA

Advisor: Brian Kish, Ph.D.

The rise of new aircraft propulsion methods (e.g., powered by batteries, fuel cells, or hybrid electric systems), the increased use of automated and integrated flight control systems, and the envisioned use of personal Vertical Take-off and Landing (VTOL) vehicles in urban environments (urban aerial mobility) lead to novel technical and regulatory challenges for aircraft manufacturers, certification authorities and operators. Of primary concern are operational safety and closely connected pilot situation awareness and workload.

The Trajectory Energy Management task involves manipulating flight and propulsion controls to achieve a planned flight profile. The key areas to focus on in Trajectory Energy Management are energy, power, and management. This research is intended to define some requirements for energy management such that the pilot can safely accomplish an intended profile and land with enough energy reserves to satisfy the intent of operation rules 91.151 (VFR reserves) and 91.167 (IFR reserves). In the context of trajectory energy management, there is a spectrum of automation tools that may assist the pilot. For example, common avionics systems with moving maps display range rings that help the pilot manage fuel state. These systems make assumptions based on current ground speed, fuel flow, and fuel reserve requirements. Requirements for similar tools that employ electric propulsion do not yet exist and must be defined based on prototype algorithm development, simulation results, and flight test data. This project provides solutions and data to help the FAA

develop performance estimation tools, flight safety assessment tools, and the associated means of compliance for Trajectory Energy Management Systems.

This research intended to develop scaling laws relating the power and energy consumption by a fixed-wing single-engine subscale model to a full-scale airplane. The research intended to relate the required power and energy consumption to achieve a planned flight profile and sustain the required power and energy consumption for individual trajectory segments. The subscale model used in this research was Albatross by Applied Aeronautics, and the full-scale airplane was Velis Electro by Pipistrel.

The power and energy demand data were collected by performing the flight tests on both aircraft with similar flight plan trajectories. The flight trajectory consisted of take-off, climb to an altitude, cruise at a constant altitude, descent, and land. Velis Electro flew with the flight mission, which included take-off, climb to a cruise altitude of 600 feet, then cruise for 10 NM at 600 feet, descent, and land. Albatross data were collected with similar flight missions but with a scaled-down cruise altitude of 160 feet.

NASA research paper [1] on "Modelling Flights" describes the geometric and dynamic similitude requirements for free-flight testing. This paper is used extensively as a reference document for calculating the model dimensions for geometric similitude and flight test profiles and environmental conditions required for dynamic similitude.

Linear scaling factors based on the wingspan, wing loading, and maximum take-off weight (MTOW) were calculated. These scaling factors were used to scale the power and rate of energy consumption by Albatross. Scaled power and rate of energy consumption were compared with the power and rate of energy consumption of full-scale airplanes. It is found in research that power and rate of energy consumption scaled using the wingspan as scaling factor had the least amount of error for the climb and cruise segment.

Table of Contents

| | |
|---|------|
| Abstract..... | iii |
| List of Figures..... | vi |
| List of Tables | vii |
| Acknowledgment..... | viii |
| Chapter 1 Motivation and Objectives | 1 |
| 1.1 Background and Objectives..... | 1 |
| 1.2 Literature Review..... | 4 |
| 1.3 Test Airplane Description | 5 |
| Chapter 2 Theory | 8 |
| 2.2 Geometric Scaling..... | 10 |
| 2.2 Dynamic Scaling | 15 |
| 2.2.1 Froude's number..... | 15 |
| 2.2.2 Reynolds Number scaling..... | 16 |
| 2.3 Power and Energy Calculations | 17 |
| 2.4 Temperature sensitivity | 20 |
| 2.6 Flight Profile | 21 |
| Chapter 3 Data Reduction..... | 22 |
| 3.1 Data Reduction..... | 25 |
| Chapter 4 Results..... | 27 |
| Chapter 5 Conclusion | 38 |
| Chapter 6 Recommendations | 39 |
| References | 40 |
| Appendix A Flight Data Analysis Tables..... | 42 |
| Appendix B Flight Data Analysis Plots..... | 45 |

List of Figures

| | |
|---|----|
| Figure 1 Pictures of Test Airplanes | 6 |
| Figure 2 Test Airplanes' dimensions comparison..... | 7 |
| Figure 3 Trajectory for Flight Tests..... | 21 |
| Figure 4 Flight plan trajectory of Velis Electro..... | 23 |
| Figure 5 Flight plan trajectory of Albatross..... | 23 |
| Figure 6 Velis Electro Flight Test Energy Consumption | 28 |
| Figure 7 Albatross Flight Test Energy Consumption | 29 |
| Figure 8 Velis Electro Altitude and Airspeed graph..... | 45 |
| Figure 9 Albatross Altitude and Airspeed graph | 46 |

List of Tables

| | |
|--|----|
| Table 1 Aircraft Specification | 7 |
| Table 2 Scale factor | 10 |
| Table 3 Dimensional Analysis | 13 |
| Table 4 Scaled Model Dimensions | 14 |
| Table 5 Scaling factor for Power and Energy | 19 |
| Table 6 Power required calculations | 19 |
| Table 7 Optimal temperature range | 20 |
| Table 8 Flight Test condition of Velis Electro and Albatross | 24 |
| Table 9 Power Consumption Comparison | 30 |
| Table 10 Energy Consumption by Velis Electro and Albatross | 31 |
| Table 11 Energy consumed in the cruise phase of the flight | 32 |
| Table 12 Rate of Energy Consumption Comparison | 33 |
| Table 13 Speed scaling | 35 |
| Table 14 Albatross Flight test trajectory | 42 |
| Table 15 Velis Electro Flight Test Data | 43 |

Acknowledgment

First and foremost, I would like to express my sincere respect and gratitude to my advisor Dr. Brian Kish for his continuous support and guidance throughout the entire research. His encouragement and kind words provided me the confidence to write my thesis. I would not have imagined having a better advisor and mentor for me.

Besides my advisor, I would like to thank Dr. Markus Wild for his constant supervision of my work progress. My sincere thanks to Dr. Brian Kish and Dr. Markus Wild for providing me with the opportunity to work on a futuristic FAA project. This project is one of the highlights of my educational and professional profession.

I would like to appreciate, Pipistrel and Applied aeronautics for providing the flight test data required for this research.

Additionally, I would like to thank the Federal Aviation Administration for sponsoring this project under contract DTFACT-17-C-00001.

Finally, I would like to thank my family for their constant support and encouragement throughout my life.

Chapter 1

Motivation and Objectives

1.1 Background and Objectives

The FAA's current regulations address energy management in terms of energy (fuel) reserves. These bases are becoming outdated because the paradigm has changed with electric propulsion, limited battery capacities, electric vehicles in the urban airspace for transportation, powertrain performance limitation due to environmental factors and temperature effects. The FAA is looking at adjusting existing regulations of Part 23 of Title 14 of the Code of Federal Regulations, specified for airplanes with a passenger-seating configuration of 19 or less and a maximum certificated take-off weight of 19,000 pounds or less, to be applicable for UAM vehicles. The main differences arise from new types of propulsion systems used. The existing civil aviation is exclusively run by internal combustion engines burning gasoline or other types of liquid carbon-based fuels.

According to 14 CFR §23.1337,

"(b) Fuel quantity indication. There must be a means to indicate to the flight crew members the quantity of usable fuel in each tank during flight. An indicator calibrated in appropriate units and clearly marked to indicate those units must be used. In addition: (1) Each fuel quantity indicator must be calibrated to read "zero" during level flight when the quantity of

fuel remaining in the tank is equal to the unusable fuel supply determined under §23.959(a);" [2]

This regulation 14 CFR §23.1337 on fuel quantity indication is not directly applicable to electrical propulsion systems. Unlike carbon-based fuels, electrical powertrains do not change the weight of the vehicle in flight, and the energy remaining cannot be measured as the volume of fuel left in a tank. Understanding the remaining energy left in the vehicle is critical at all times of flight to ensure that a safe landing can be performed at any given moment. The definition of remaining fuel and how to present this information to the pilot requires an update. It is necessary to understand the electric energy consumption in a flight envelope and within each flight phase. It is essential to understand the factors affecting the power-trains performance to define usable fuel.

The new developing electric airplanes have unique designs and technology. It is required to understand the energy consumption during each phase of flight, starting from take-off, climb, cruise, descent, and landing for these designs. To estimate the battery energy requirement to fly from point A to point B for every design technology is a tricky task. Instead of developing a full-scale prototype in the initial design phases, a subscale prototype can study its characteristics. Then, the subscale airplanes can apply to scale laws to estimate the full-scale airplane's power and energy requirements.

The mathematical models do not have full liberty to model real-time environmental conditions correctly, model the battery temperature change with flight trajectory, and model the motor and inverter effects. Integrating the power train model with the environmental effect to correctly predict the energy consumption will be a little tricky.

NASA has been using the scaled model for aerodynamic data gathering in wind tunnel tests, problem-solving exercises for vehicles in production, and proof of aeronautical concepts. In this study, a scaled and full-scale airplane is used to study power and energy demands in different parts of flights. The results from both the test airplanes are compared for power and energy consumption. The scaling factors were used to relate the power and energy consumption between these airplanes.

The power required for an airplane is dependent on the wingspan, wing loading, and MTOW of the airplane. These parameters were then used as scaling factors to relate the subscale's power to the full-scale airplane. Next scaling factors were used to scale the electric power and rate of energy consumption for the subscale airplane to a full-scale airplane.

Geometric similitude was established using dimensional analysis. The environmental conditions required for flight testing were established using the dynamic similitude requirements. Power and energy were calculated using the formulas used in aerospace and electrical systems. The real-time flight test data were collected from Albatross, representing the subscale model and Velis Electro for the full-scale airplane. The test data from these two airplanes were used for validating the scaling laws.

The scaling factors used here can be applied to a similar type of subscale electric aircraft to estimate its full-scale version's power and energy requirements. These scaling factors can further estimate the battery weight and specific energy density required for a full-scale airplane.

1.2 Literature Review

Although the Concept of electric airplanes is not new to history, there is not much literature available on electric energy consumption during each phase of the flight. Studies have compared the specific energy of jet fuel, kerosene oil, fuel cell, and electric battery. Martin Hepperle [3], in his paper, compared the efficiency of components used in the turboprop, turbofan, battery, and fuel cell. Then compared the equivalent energy density of propulsion systems providing a shaft power of 50 kW for 2 hours.

The propulsion systems' component sizing trends were compared in [4] by analyzing commercial off-the-shelf (COTS) available electric motors, inverters, and rotors targeted for the eVTOL aviation market. The analysis is done by creating a database with the component specifications and comparing the automotive industry data. This study presents graphs showing the trends in weight Vs. Power for liquid-cooled and air-cooled motors and inverters used in the automotive industry and aerospace industry.

A battery model in [5] aims to estimate the size and capacity of battery requirements by introducing the battery model into the existing aircraft sizing and flight simulation environment for Ce-Liner and proposes a simplified approach for battery capacity estimation for a standard mission profile.

Background information on methods of dynamic and free flight-testing on subscale models were introduced in [1]. It acknowledges the importance of testing the subscale model for the character analysis of a full-scale aircraft. Scaling laws for calculating the dimensions of subscale aircraft are presented for compressible and incompressible flow.

A mission planning tool (MPT) that models aerodynamic, propulsion, and electric systems of NASA Maxwell X-57 is developed [6]. This tool simulates and captures the

performance parameters for all flight phases: taxi, take-off, climb, cruise, and descent. This study also presents the results of battery temperature, motor temperature, motor power, and SOC for each flight phase.

Literature research produced here focuses on the battery pack design, comparing different types of fuels, design challenges with complex control systems associated with new types of electric vehicles. Not much of research is involved in using subscale models for estimating the energy and power consumption profile. The research in the area of electric powertrain power and energy consumption for each flight phase is not available.

1.3 Test Airplane Description

Velis Electro, shown in Figure 1, is a two-seat side-by-side, high fixed-wing, single-engine, fully electric, light aircraft with a T-tail configuration airplane. The single electric motor is in tractor configuration. The airframe is made of Carbon Fiber and Kevlar composites. The propulsion sub-systems consist of Pipistrel E-811 electric motor, two Pipistrel PB345V124E-L 345 VDC 11.0kWh lithium batteries, its version of BMS (monitoring the health of battery), an inverter/controller, and three-bladed composite fixed pitch propeller P-812-164-F3A. The propulsion sub-systems are liquid-cooled. It is

intended for pilot training and manufactured by Pipistrel; a company based in Slovenia. The aircraft is type certified (EASA.A.573 TCDS) [7]



1.a.) Pipistrel Velis Electro

1.b.) Albatross by Applied Aeronautics

Figure 1 Pictures of Test Airplanes

Albatross, shown in Figure 1, is a fully autonomous, high fixed-wing, single-engine, full electric UAV with a fiberglass body. It is manufactured by Applied Aeronautics, headquartered in Austin, Texas. It has a pusher-prop with an inverted v-tail design. It has a Scorpion 4020-420KV Motor, Castle Creations Phoenix Edge 100 electronic speed controller, 21.4 Volt battery pack, and two-blade propellers. Autopilot is from Pixhawk. This UAV can fly in both manual and autonomous mode. It uses "QGroundControl" software for mission planning and execution. Figure 2 is a pictorial representation comparing dimensions of Velis Electro and Albatross.

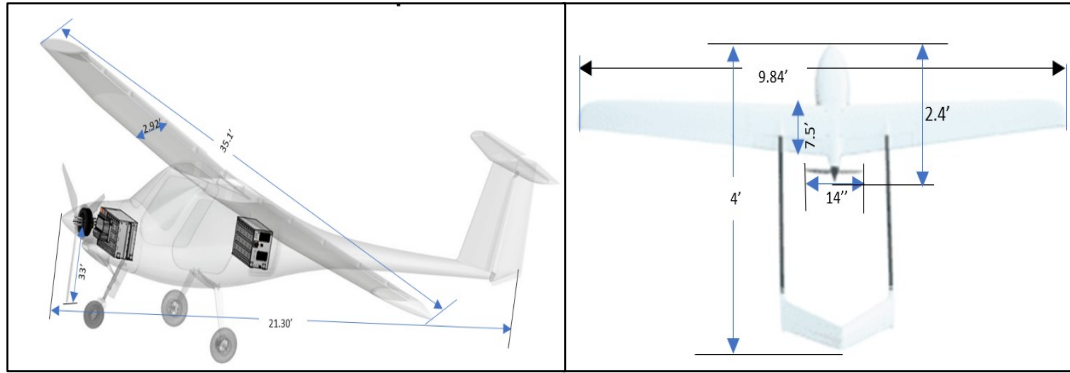


Figure 2 Test Airplanes' dimensions comparison

Table 1 Compares the trajectory related specifications of test airplanes.

Table 1 Aircraft Specification

| | Velis Electro | Albatross |
|--------------------------------|----------------------|-------------------------|
| MTOW (lbs.) | 1320 | 22.5 |
| Flight Time (min.) | 60 | 60 |
| Wingspan (ft.) | 35.10 | 9.84 |
| Glide Ratio | 15:1 | 30:1 |
| Max. Range (NM) | 75 | 21.59 |
| Max. Altitude (MSL) | 12800 | 2000 |
| Payload (lb.) | 378 | 9.70 |
| Battery Energy Density (Wh/kg) | 291 [8] | 261 [9] |
| Battery Capacity (KWh) | 21 | 0.34 |
| Cruise Speed (mph) | 119 | 42 |
| Engine | Pipistrel E-811 | Scorpion SII-4020-630KV |

Chapter 2

Theory

Certain similitude requirements should be met between the model and full-scale airplane to apply the data obtained from subscale model flight tests to a full-scale aircraft with maximum validity. The similitude of the geometric configurations is a fundamental requirement, as is the similitude Reynolds number and Froude number in incompressible flow conditions. The technique of dynamic free-flight testing was used in this research. In this technique, a powered or unpowered model is flown without appreciable restraint in wind tunnels or outdoor test ranges. [1]. The structure of the model is a rigid body and does not have aeroelastic effects. Dynamically similar replicas are specifically designed to replicate geometry and motion between subscale and full-scale vehicles. A geometrically similar model of an aircraft reacts to external forces and moves in such a manner that the relative positions of its components are geometrically similar to those of a full-scale airplane [1].

Geometric scale requirements for the model, such as the wingspan, length, chord length, wing area, scale ratio of force, mass, and time, are maintained between the model and the full-scale airplane for dynamic similitude. This thesis attempts to prove that a dynamical subscale electric airplane with a subscale flight profile will follow a similar energy consumption profile as a scaled-up airplane.

The airflow was considered incompressible, as the tests were conducted at low altitudes (less than 5000 ft.), the air has a higher density, and airplane speed was less than 200 mph. The structure of a full-scale airplane is made with a composite of carbon fiber and Kevlar

[10]. Typically, the carbon fiber density is 125 lbs./ft.³, and Kevlar is 87 lbs./ft.³. The composite of both of these materials will have a density between 87 to 125 lbs./ft.³. The structure of the model airplane is made with fiberglass, and its density is 125 lbs./ft.³. The ratio of the density of the material used in the airframe of the subscale model and the full-scale airplane is approximately the same.

The scale factor (N), also known as the linear scale ratio between the model and the full-scale airplane, was calculated using the wingspan, wing loading, and MTOW. These three parameters were chosen for scaling as the power required is directly proportional to these three parameters. Also, the Model (Albatross) used for collecting the flight test data is not a perfectly scaled-down version of the full-scale airplane (Velis Electro). Scaling factors calculated using wingspan, wing loading, and MTOW were used to calculate the ideal model dimensions and also used in calculating the scaled power and rate of energy consumption calculation.

In Table 2, the scaling factor based on the wingspan is calculated by taking the ratio of the wingspan of Velis Electro and the wingspan of the Albatross. This wingspan scaling factor is later used in calculating the dimensions of a model with the wingspan as a scaling factor in Table 4. Similarly, the scaling factor based on wing loading is calculated by dividing the wing loading of Velis Electro by wing loading of Albatross in Table 2. This wing loading scaling factor is later used in calculating the dimensions of a model with wing loading as scaling factor in Table 4. The scaling factor based on MTOW is calculated by equating the ratio of the MTOW of Velis Electro by MTOW of Albatross to the cube of scaling factor. This MTOW scaling factor is later used in calculating the dimensions of a model with MTOW as the scaling factor in Table 4.

Table 2 Scale factor

| | | |
|--------------|--|--|
| Wingspan | $\frac{(\text{wingspan})_{fs}}{(\text{wingspan})_m}$ | $N = \frac{35.1}{9.81} = 3.57$ |
| Wing Loading | $\frac{(\text{wing loading})_{fs}}{(\text{wing loading})_m}$ | $N = \frac{12.89}{3} = 4.3$ |
| MTOW | $\frac{(\text{MTOW})_{fs}}{(\text{MTOW})_m}$ | $N^3 = \frac{1320}{22.05} = 59.86$ $N = 3.91$ |

2.2 Geometric Scaling

Each characteristic of a model can be related to its corresponding characteristic of the full-size airplane employing a scale factor. A model and full-size article are geometrically similar if all body dimensions in all three coordinates have the same linear scale ratio. All angles are preserved in geometric similarity, and all flow directions are preserved.

The method of dimensional analysis was used in determining the proportionality factor to calculate the model dimensions. Physical quantities of interest are expressed in terms of three fundamental dimensions: mass (M), length (L), and time (T) in column "Dimensional analysis" of Table 3.

Although Reynolds number is a dimensionless quantity, here, it is used as an example for breaking a physical quantity into base units. ρ is density, V is velocity, x is characteristic length, η is dynamic viscosity. Expressing Reynolds number (R_e) in terms of the three basic units of length, mass, time as:

$$R_e = \frac{\rho * V * x}{\eta} \quad \text{Equation 1}$$

$$R_e = \frac{[M^1 L^{-3} T^0] * [M^0 L^1 T^{-1}] * [L^1]}{[M^1 L^{-1} T^{-1}]} \quad \text{Equation 2}$$

$$R_e = [M^0 L^0 T^0] \quad \text{Equation 3}$$

Similarly, the method of dimensional analysis was used in calculating the base units of the other physical parameters required for geometric scaling are listed in Table 3.

Dimensional proportionality for velocity is calculated in the next few equations starting with the lift equation:

$$Lift = \frac{1}{2} \rho V^2 S C_L \quad \text{Equation 4}$$

For steady level flight:

$$Lift = Weight \quad \text{Equation 5}$$

The model and the full-scale airplane were to be tested at an altitude of less than 4000 feet; the relative density factor is taken as 1. The model and full-scale airplane are tested in the

same gravitational field, and therefore linear accelerations are equal between the model and full-scale airplane. As lift and weight are forces, and forces are proportional to Length³. ρ is the density which is proportional to 1. S is the area that is proportional to Length².

$$L^3 \propto 1 \cdot 1 \cdot V^2 \cdot L^2 \quad \text{Equation 6}$$

$$V^2 \propto L \quad \text{Equation 7}$$

$$V \propto \sqrt{L} \quad \text{Equation 8}$$

Dimensional proportionality for time is calculated as follows:

$$\text{Time} = \frac{\text{Distance}}{\text{velocity}} = \frac{L}{V} = \frac{L}{\sqrt{L}} = \sqrt{L} \quad \text{Equation 9}$$

From the above Equation 8 and Equation 9, it is established that velocity and time are proportional to \sqrt{L} . The base units of mass, length, and time are then converted in terms of length by replacing mass with L³ and time with \sqrt{L} in Table 3. The proportionality factor in Table 3 is then expressed in terms of scaling factor (N). The scaling ratio to calculate the wingspan, wing loading, and MTOW of the model airplane are also present in Table 3.

Table 3 Dimensional Analysis

| Parameter | Dimensional analysis | Proportionality in terms of length | Scaling Factor |
|--|-----------------------|------------------------------------|----------------------|
| Relative Density | $[M^1 L^{-3} T^0]$ | 1 | 1 |
| Linear acceleration | $[M^0 L^1 T^{-2}]$ | 1 | 1 |
| Time | $[M^0 L^0 T^1]$ | $L^{1/2}$ | \sqrt{N} |
| Velocity | $[M^0 L^1 T^{-1}]$ | $L^{1/2}$ | \sqrt{N} |
| Wing Area | $[M^0 L^2 T^0]$ | L^2 | N^2 |
| Volume | $[M^0 L^3 T^0]$ | L^3 | N^3 |
| Force | $[M^1 L^1 T^{-2}]$ | L^3 | $\frac{N^3}{\sigma}$ |
| Wingspan | $[M^0 L^1 T^0]$ | L^1 | N |
| Wing Loading | $[M^1 L^{-1} T^{-2}]$ | L^1 | N |
| Mass, weight | $[M^1 L^0 T^0]$ | L^3 | $\frac{N^3}{\sigma}$ |
| <p>Where σ is the ratio of the air density to that at sea level (ρ/ρ_0), and ν is the ratio of kinematic viscosity of the air to that at sea level $\frac{\nu}{\nu_0}$. Model airplane's dimensions can be calculated by dividing the full-scale airplane's dimensions by the indicated scale factor.</p> | | | |

The model airplane used for the flight tests is not a perfect geometric subscale model of the full-scale aircraft Velis Electro. Multiple geometric subscale models' dimensions were calculated using the linear scaling factor ratio developed using the wingspan, wing loading, and MTOW in Table 2 and dimensional analysis relations set in Table 3. The albatross dimensions were then compared with the ideal model dimensions calculated using wingspan,

wing loading, and MTOW as scaling factor in Table 4. It can be observed from Table 4 that aspect ratio, a dimensionless number for geometric similarity, is approximately the same for all three ideal models and Velis Electro. The aspect ratio of Albatross is comparatively higher. The chord length of ideal model calculated with MTOW as scaling factor is same as Albatross.

Table 4 Scaled Model Dimensions

| Dimensions | Velis Electro (Full-scale airplane) | Albatross (Model used in flight test) | Ideal model with wingspan as scaling factor (N = 3.57) | Ideal Model with wing loading as scaling factor (N = 4.3) | Ideal Model with MTOW as scaling factor (N = 3.91) |
|-------------------------------|-------------------------------------|---------------------------------------|--|---|--|
| Fuselage length (ft.) | 21.3 | 2.43 | 5.97 | 4.95 | 5.44 |
| Wing area (ft. ²) | 102.4 | 7.36 | 8.05 | 5.54 | 6.69 |
| Aspect ratio | 12.4 | 13.16 | 12.03 | 12.03 | 12.03 |
| Chord Length (ft.) | 2.92 | 0.75 | 0.82 | 0.68 | 0.75 |
| Wingspan (ft.) | 35.1 | 9.84 | 9.84 | 8.16 | 8.97 |
| Wing Loading (lb./ ft.2) | 12.89 | 3 | 3.61 | 3 | 3.3 |
| MTOW (lb.) | 1320 | 22.05 | 29.11 | 16.60 | 22.05 |

2.2 Dynamic Scaling

NASA's report on dynamic similitude [11] for the general test conditions explains the dimensionless number requirements for different flight test circumstances. Four dimensionless numbers, namely Reynolds number, Mach number, Froude number, Strouhal number, are used for dynamic similitude. It is difficult to satisfy all of the similitude conditions. So, most of the flight tests are designed for certain similitude conditions at the expense of other parameters.

NASA report [1] and [11] are used to determine the dimensionless number required for dynamic and kinematic similitude for flight test in this thesis. The kinematic properties are preserved by using velocities scaled from the Froude number. And dynamic similitude using the Reynolds number.

2.2.1 Froude's number

Froude's number (Fr) must be equal for the model and full-scale airplane to assure similitude of inertial and gravitational effects on maneuvering vehicles having geometric similitude. The aircraft will exhibit similar flight behavior for the same angle of attack and dynamic motions. Froude number can be expressed as follows:

$$Fr = \frac{v}{\sqrt{gL}} \quad \text{Equation 10}$$

Equating the Froude number of the model and full-scale airplane to calculate the velocity relation:

$$(Fr)_m = (Fr)_{fs} \quad \text{Equation 11}$$

$$\left(\frac{V}{\sqrt{gL}}\right)_m = \left(\frac{V}{\sqrt{gL}}\right)_{fs} \quad \text{Equation 12}$$

$$(V)_m = \left(\frac{L_m}{L_{fs}}\right)^{\frac{1}{2}} (V)_{fs} \quad \text{Equation 13}$$

Where V is velocity, g is gravitational acceleration, L is the characteristic length, m is for model, and fs is for full scale. The model's velocity is equal to the full-scale airplane velocity divided by the length ratio's square root (scaling factor).

2.2.2 Reynolds Number scaling

Reynolds number is a ratio of the fluid's inertia forces to the fluid's boundary layer's viscous forces. For dynamic similitude, the model and full-scale airplane should fly with the same Reynolds number. Reynolds number can be written as:

$$R_e = \frac{\rho V x}{\mu} \quad \text{Equation 14}$$

In the above equation, ρ is the density of the medium (air), V is the airplane's velocity, x is characteristic length (Chord length of the wing), μ is the medium's viscosity.

It is challenging to have the same Reynolds number for subscale and full-scale airplanes. The subscale model (Albatross) is restricted to fly at an altitude of 400 ft. MSL and the maximum cruise speed of 70 knots. The full-scale airplane (Velis Electro) used in flight

test can fly up to 12000 ft MSL and minimum stalling speed of 45 knots. The characteristic length (Chord length) of the Velis Electro is 3.5 times of Albatross. So, it is impossible to get the same Reynolds number for Albatross and Velis Electro.

The velocity relation between the model (m) and full-scale (fs)airplane was established using the same Froude's number in section 2.2.1. Reynolds number relationship is established by taking the ratio of Reynolds number of model and full-scale airplane:

$$\frac{Re_m}{Re_{fs}} = \frac{V_m x_m}{v_m} * \frac{v_{fs}}{V_{fs} x_{fs}} \quad \text{Equation 15}$$

Then insert the value of velocity from Froude's scaling Equation 13 into Equation 15:

$$\frac{Re_m}{Re_{fs}} = \left(\frac{L_m}{L_{fs}} \right)^{\frac{3}{2}} * \frac{v_{fs}}{v_m} \quad \text{Equation 16}$$

Equation 16 is used to find the Reynolds number relation between the model and the full-scale airplane. In NASA paper [1] also, for incompressible flow with the same Froude's number between the model and full scale, the Reynolds number is scaled using Equation 16.

2.3 Power and Energy Calculations

Calculated the relationship of wingspan, wing loading, and MTOW with the power required for a level flight as follows:

$$W = L = \frac{1}{2} \rho V^2 S C_L \quad \text{Equation 17}$$

$$V = \left(\frac{2mg}{\rho S C_L}\right)^{1/2} = \left(\frac{2w_s g}{\rho C_L}\right)^{1/2} \quad \text{Equation 18}$$

$$P_{req} = DV = \frac{1}{2}\rho V^3 S C_{D_o} + \frac{W^2}{\frac{1}{2}\rho V S} \left(\frac{1}{\pi e AR}\right) \quad \text{Equation 19}$$

By inserting the value of velocity from Equation 18 in Equation 19 and rearranging the parameters for P_{req} :

$$P_{req} = \left(\frac{2w_s^3 g^3}{\rho}\right)^{\frac{1}{2}} S \left(\frac{C_{D_o}}{C_L^{\frac{3}{2}}} + \frac{C_L^{\frac{1}{2}}}{\pi e AR}\right) \quad \text{Equation 20}$$

Where w_s is wing loading, S is wing area, AR is the aspect ratio. It is obtained that the power required is directly proportional to wing area, wing loading, and MTOW.

Power, energy, and rate of energy consumption can be broken down into the base unit of mass, length, and time Table 5. The scaling factor for power, energy, and rate of energy consumption is calculated in Table 5 using the relations established in the previous sections. Dimensional analysis of Equation 20 will also result in the same base units for power required.

Table 5 Scaling factor for Power and Energy

| Parameter | Dimensional analysis | Linear relation | Scaling Factor |
|----------------|----------------------|-----------------|----------------|
| Power | $[M^1 L^2 T^{-3}]$ | $L^{7/2}$ | $N^{3.5}$ |
| Energy | $[M^1 L^2 T^{-2}]$ | L^4 | N^4 |
| Rate of Energy | $[M^1 L^2 T^{-3}]$ | $L^{7/2}$ | $N^{3.5}$ |

The power required in Table 6 were calculated using Equation 20 for models with ideal dimensions, Albatross and Velis Electro (dimensions calculated in Table 4). The power required by models with ideal dimensions and Albatross were scaled up using the scaling factors calculated in Table 5. These scaled powers were then compared with the power required by Velis Electro. The error is calculated using Equation 21. Power required for Velis Electro is 442235.7 lb.ft.²/s³ and power required for model is 3560.4 lb.ft.²/s³.

$$\text{Error in } P_{req} = \frac{[(P_{req})_{fs} - ((P_{req})_m * N^{3.5})] * 100}{(P_{req})_{fs}} \quad \text{Equation 21}$$

Table 6 Power required calculations

| | Scale Factor | P_{req} with Ideal Model | Error in P_{req} with Ideal Model | Error in P_{req} with Albatross |
|--------------|--------------|----------------------------|-------------------------------------|-----------------------------------|
| Wingspan | 3.57 | 5163.6 | 0 | 30.8 |
| Wing Loading | 4.3 | 2682.3 | 0.0 | -32.7 |
| MTOW | 3.91 | 3734.7 | 0.0 | 4.7 |

In Table 6, "P_{req}" with Ideal model" is the power required calculated using the ideal model dimensions with the respective scaling factor, "Error in P_{req}" is calculated using Equation 21.

From Table 6, it is clear that with ideal model dimensions, the power required can be scaled with 0% errors. With ideal model dimensions, estimating a full-scale plane's power and energy requirements will have almost 0 % errors irrespective of the scaling factor used. Any one of wingspan, wing loading, or MTOW can be used as a scaling factor. On the other hand, Albatross has inherent power required errors in the range of $\pm 35\%$.

2.4 Temperature sensitivity

The operating temperature range for electric propulsion systems is a subject of great interest, as each subsystem's performance is sensitive to change in temperature. The optimal temperature range of motor, battery, and inverter operation is present in Table 7.

Table 7 Optimal temperature range

| Component | Temperature Range (deg. C) |
|------------------|--|
| Battery | The acceptable temperature range is 20°C – 60°C The optimal temperature range is 15°C – 35°C [12] |
| Motor | Motor's internal temperature rise depends on the type of insulation used, and the ambient temperature of less than 40°C is considered to be optimal. |
| Inverter | At an ambient temperature of less than 37°C, inverter efficiency is in the range of 95 to 96%. And it decreases by 2.5% at a higher temperature range [13] |

The flight tests on Albatross and Velis Electro were performed in the normal operating range. OAT during the flight tests performed on the Velis Electro was 29 degrees Celsius, and Albatross was 24 degrees Celsius.

2.6 Flight Profile

The flight test profile consisted of take-off, initial climb to 35 ft., climb, cruise (level flight), descent, and landing. As the subscale airplane used is a UAV, the operating rules

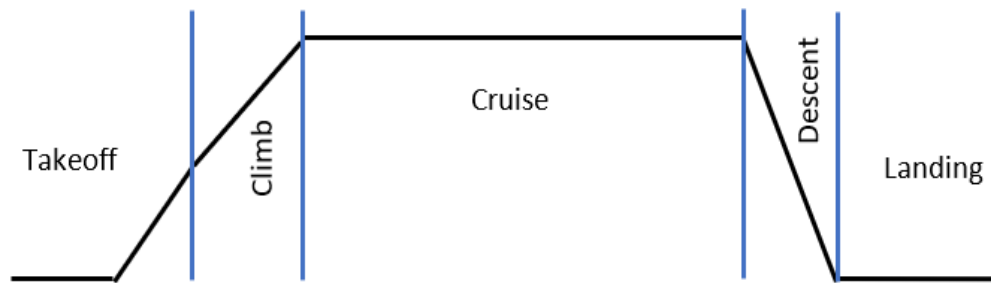


Figure 3 Trajectory for Flight Tests

listed in the 14 CFR are followed. As per the CFR § 107.51(b) [14], the maximum cruise altitude is limited to 400 ft. and is limited to fly in line of sight. The model airplane is approximately 3.5 times smaller than the full-scale airplane. The flight profiles are also scaled in this ratio. As dimensionally, altitude is having a unit of length (L). The profile altitude is scaled proportionally to N. The velocity is to be scaled according to the relationship developed between the velocity and length using Froude's number in Equation 13.

Chapter 3

Data Reduction

Full-scale flight test data were collected from fixed-wing single-engine electric propulsion Velis Electro. It was provided by Pipistrel, the manufacturer of Velis Electro. The data log provided was in the ".csv" file format. The data log included battery state parameters such as SOC, battery current, battery voltage, battery cell temperature, engine parameters such as motor power, motor RPM, requested torque, motor temperature, and flight plan parameters such as IAS, altitude, OAT, Latitude, longitude.

Albatross flight test data were provided by its manufacturer Applied Aeronautics in the format of "filename.Ulog". The file format used by Pixhawk autopilot software. The test flight log file can be uploaded on their website [15] to generate a trajectory in 3D. Python is used to convert the "ulog" file format to readable ".csv" format with the help of the method explained on the webpage [16]

Figure 4 shows the flight plan trajectory of Velis Electro. MATLAB was used to generate the flight plan trajectory of Velis Electro using the Latitude and longitude coordinates.

Figure 5 shows the flight plan trajectory of Albatross generated using the Pixhawk review tool [15].



Figure 4 Flight plan trajectory of Velis Electro



Figure 5 Flight plan trajectory of Albatross

Details of flight test conditions of Velis Electro and Albatross are presented in Table 8. The flight trajectory of Velis Electro was take-off, climb to a cruise altitude of 600 feet, then cruise for 10 NM at 600 feet, descent, and land. The indicated airspeed at cruise was 89 knots for Velis Electro. The flight mission of Albatross was collected with a similar flight mission as Velis Electro but with a scaled-down cruise altitude of 160 feet. The cruise speed was 37 knots for Albatross.

Table 8 Flight Test condition of Velis Electro and Albatross

| AIRCRAFT | Velis Electro | Albatross | AIRCRAFT | Velis Electro | Albatross |
|--------------------------|-----------------|----------------|-----------------------|---------------|-----------|
| Test Location | Gorizia Airport | Wisconsin, USA | Cruise altitude (ft.) | 633 | 161 |
| Test Date | 09/23/2020 | 07/02/2019 | Cruise Speed (Knots) | 89 | 37 |
| MTOW (lbs.) | 1,320 | 22 | Flight Time (Min.) | 24 | 8.26 |
| OAT (°C) | 29 | 24 | Energy Consumed (kWh) | 8.11 | 0.04 |
| Cruise length (NM) | 10 | 4.11 | Max Power (kW) | 60 | 1.5 |
| Test Location AMSL (ft.) | 207 | 1525 | | | |

The tests on both airplanes were performed in the normal temperature operating range of the powertrain. The effects of temperature on the performance of the powertrain are not studied in this thesis. The maximum power drawn for both the airplane was in the take-off phase during lift-off from the ground.

3.1 Data Reduction

Once all the test data are recorded and collated, a step-by-step data reduction methodology is applied. All the steps explained here are applied to flight test data recorded from Velis Electro and Albatross. First, the sample time is reduced for the data as both the test articles' data were in nanoseconds. The timestamp is converted from nanoseconds to minutes. Then data with a 0.01-minute interval was retained for analysis. Then parameters such as instant energy consumption, energy consumption, power, and rate of energy consumption were calculated using the following formulas:

$$\mathbf{Power} = \frac{\mathbf{Voltage*Current}}{\mathbf{1000}} \quad \mathbf{Equation\ 22}$$

$$\mathbf{Instat\ Energy} = \frac{\mathbf{Voltage*Current*time_{minutes}}}{\mathbf{60*1000}} \quad \mathbf{Equation\ 23}$$

$$\mathbf{Energy} = \frac{\mathbf{Voltage*Used\ Capacity}}{\mathbf{1000}} \quad \mathbf{Equation\ 24}$$

$$\mathbf{Rate\ of\ Energy\ consumption} = \frac{\mathbf{Total\ Energy\ consumed}}{\mathbf{Time\ period}} \quad \mathbf{Equation\ 25}$$

The battery used capacity in the model is given in terms of a milliampere-hour. The used capacity is the sum of all the discharged electric charges until that point. Used capacity in

Velis Electro was calculated by multiplying the Current*(time period). Units used for instantaneous energy is Wh, energy consumption is kWh, and power is kW.

After this, the flight test's data sets were split into individual flight phases for further analysis (see Appendix A Table 14, Table 15). Flight phases included for analysis were take-off (ground roll and initial climb to 35 ft.), climb, cruise, descent, and landing. The individual flight phases based on the parameter are then either averaged or subtracted from previous phase data. The average was taken for parameters such as IAS, voltage, current, and power, etc. Subtraction was done for phase duration, SOC, used capacity, flight time, battery remaining, altitude, etc. Then these data were compared to get an overall view of each flight phase. This allowed identifying phases with the highest power draw and energy consumption. These results were then compared between the model and the full-scale airplane.

It was observed that power required scaled using any of the scaling factors produces almost zero percent errors with the ideal model dimensions in Table 6. The Albatross is not a correct subscale version of Velis Electro, so the power and rate of energy consumption of Albatross were scaled using all three scale factors wingspan, wing loading, and MTOW. It was done to validate which scaling factors work best for flight test data used in this study.

Chapter 4

Results

The objective of developing scaling laws relating to power and energy consumption between the scaled and full-scale airplanes was achieved. It was achieved by comparing and analyzing the power drawn, energy consumption, and rate of energy consumption and splitting it into particular flight phases. First, we analyzed the individual flight profile data of Albatross and Velis Electro, and then it was compared to each other using the scaling factors.

The flight trajectory (see Appendix B, Figure 8) flown by Velis Electro and (see Appendix B, Figure 9) flown by Albatross maintained approximately a constant altitude and airspeed during the cruise phase. The above-ground cruise altitude of Velis Electro is approximately 3.5 times the Albatross cruise altitude.

In Figure 6 and Figure 7, the power drawn at take-off is the highest. At take-off, excess thrust is required to generate lift, gain altitude and overcome the drag, which in turn increases power demand from batteries. Motors are required to run on high RPM. During the climb phase, the energy consumption rate is higher than in the cruise phase, observed from the slope of energy consumption in Figure 6 and Figure 7, and the rate of energy consumption in Table 12. The rate of energy consumption in the climb phase for Albatross is 2.69 Wh/min, and for Velis Electro, 336 Wh/min higher than the cruise phase.

During the cruise phase, the power demand decreases as the Velis Electro and Albatross are flying at an approximately constant speed. Figure 6 for Velis Electro, the power draw

is consistent for a few minutes into the descent phase as the airplane is losing altitude, but it is still flying at the same speed as it was flying in the cruise segment. In Figure 6 and

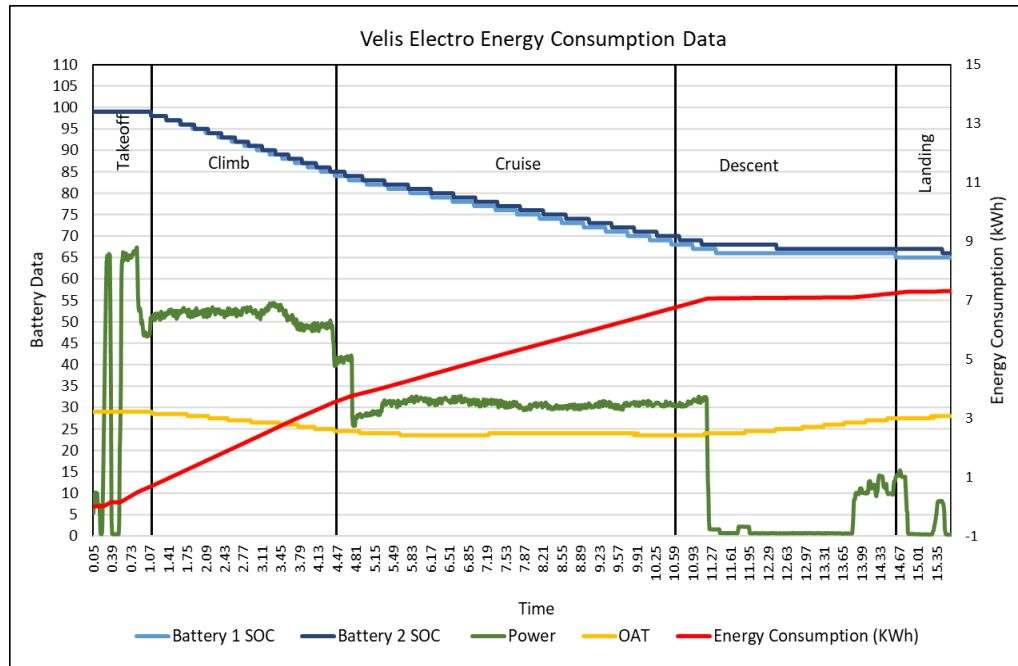


Figure 6 Velis Electro Flight Test Energy Consumption

Figure 7, power demand decreases during the descent and landing phases. During these phases, less thrust is required, in turn, less power draw and less load on the motor and inverter. In Figure 6 for Velis Electro, there is a slight increase in the power drawn just before the landing. In Figure 6, the energy consumption and SOC lines are almost parallel to the horizontal axis, indicating a decrease in energy consumption in the descent and landing phase.

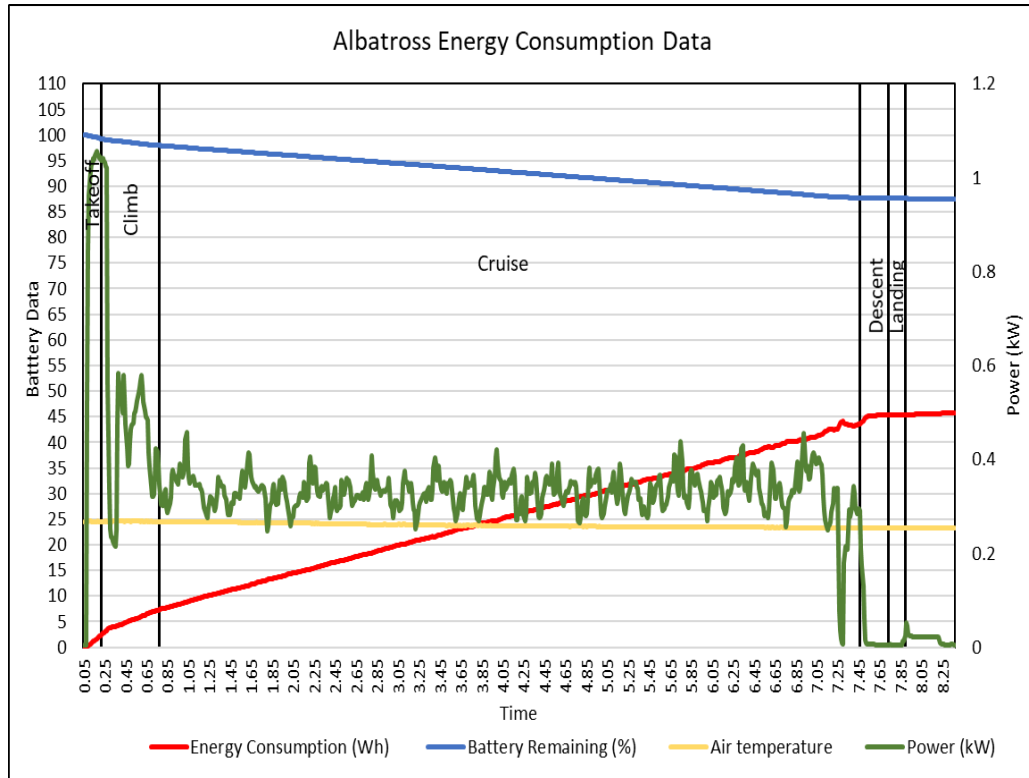


Figure 7 Albatross Flight Test Energy Consumption

From Equation 28, it can be concluded that the power required (P_{req}) is directly proportional to the wing loading, wingspan and inversely proportional to the aspect ratio. Wing loading is the ratio of MTOW and wing area.

In Table 9, the power draw for each phase of the flight is calculated for Velis Electro and Albatross. For each flight phase, the power draw from Albatross was scaled up using the wingspan, wing loading, and MTOW scaling factors. These values were then compared with the power draw from Velis Electro. The error in power was calculated by comparing the scaled data from Albatross with the power data of Velis Electro. The power error in Table 9 is calculated using Equation 22.

Table 9 Power Consumption Comparison

| | Power Velis Electro (kW) | Power Albatross (kW) | Scaled Error (N = 3.57) (%) | Scaled Error (N = 4.3) (%) | Scaled Error (N = 3.91) (%) |
|-------------------------|-------------------------------------|-----------------------------|------------------------------------|-----------------------------------|------------------------------------|
| Takeoff (Ground roll) | 37.42 | 0.85 | -95.28 | -274.50 | -168.49 |
| Takeoff (Initial Climb) | 49.03 | 1.05 | -84.11 | -253.08 | -153.13 |
| Climb | 51.33 | 0.50 | 16.26 | -60.60 | -15.14 |
| Cruise | 31.13 | 0.33 | 8.87 | -74.77 | -25.30 |
| descent | 7.44 | 0.01 | 88.45 | 77.84 | 84.11 |
| Landing | 4.33 | 0.01 | 80.15 | 61.92 | 72.70 |

The energy consumption during each phase of flight is calculated in Table 10. The cruise segment length of Velis Electro was 10 NM. The cruise segment length based on wingspan, wing loading, and MTOW as scaling factors the Albatross should have cruise

segment length of 2.80 NM, 2.33 NM, 2.56 NM, respectively. The flight test data available for Albatross did not have the scaled cruise segment length. The rate of energy consumption was used to estimate the amount of energy required for scaled cruise segments. The comparison of scaled-up energy consumption in take-off, climb, descent, and landing phase is present in Table 10. The comparison of scaled-up energy consumption for the cruise segment is present in Table 11.

Table 10 Energy Consumption by Velis Electro and Albatross

| Unit Energy- Wh | Energy Consumption Velis Electro | Energy Consumption Albatross | Scaled Error (N = 3.57) (%) | Scaled Error (N = 4.3) (%) | Scaled Error (N = 3.91) (%) |
|-------------------------|---|---|--|---------------------------------------|--|
| Takeoff (Ground roll) | 508.15 | 1.33 | 57.49 | 10.52 | 39.45 |
| Takeoff (Initial Climb) | 192.26 | 0.88 | 25.65 | -56.48 | -5.89 |
| Climb | 2878.7 | 4.57 | 74.21 | 45.73 | 63.27 |
| Cruise | 3190.7 | 36.60 | | | |
| descent | 496.19 | 0.08 | 97.38 | 94.49 | 96.27 |
| Landing | 71.97 | 0.02 | 95.49 | 90.50 | 93.57 |

The error in the scaled-up energy consumption from Albatross to Velis Electro was calculated using Equation 26:

$$\text{Error in } E = \frac{[(E)_{fs} - (E)_m * N^4] * 100}{(E)_{fs}} \quad \text{Equation 26}$$

Where E is energy consumption, N is the scaling factor, m is for the model, and fs is full scale.

In Table 11, the energy consumed by Albatross for the cruise segment is calculated for all three scaling factors. The percentage of energy consumption error is calculated by comparing it with full-scale airplane energy consumption in the cruise phase.

Table 11 Energy consumed in the cruise phase of the flight

| | Energy consumed Albatross (Wh) | Energy Error (%) |
|-----------------|--------------------------------|------------------|
| Cruise (N=3.57) | 25.71 | -31 |
| Cruise (N=4.3) | 20.79 | -125 |
| Cruise (N=3.9) | 22.97 | -67 |

In Table 12, the rate of energy consumption for each phase of the flight is calculated for Velis Electro and Albatross. For each flight phase, the rate of energy consumption from Albatross was scaled up using the wingspan, wing loading, and MTOW scaling factors. These values were then compared with the rate of energy consumption from Velis Electro. The error in the rate of energy consumption was calculated by comparing the scaled data from Albatross with Velis Electro's energy consumption data.

An error in the scaled rate of energy consumption from Albatross to Velis Electro was calculated using Equation 27:

$$\text{Error in } E_r = \frac{[(E_r)_{fs} - (E_r)_m * N^{3.5}] * 100}{(E_r)_{fs}} \quad \text{Equation 27}$$

Where E_r is the rate of energy consumption, N is the scaling factor, m is for the model, and fs is full scale.

Table 12 Rate of Energy Consumption Comparison

| | Rate of Energy Consumption Velis Electro (Wh/min) | Rate of Energy Consumption Albatross (Wh/min) | Scaled Error (N=3.37) (%) | Scaled Error (N=4.3) (%) | Scaled Error (3.91) (%) |
|-------------------------|--|--|---------------------------|--------------------------|-------------------------|
| Takeoff (Ground roll) | 623.73 | 14.76 | -103.44 | -290.15 | -179.71 |
| Takeoff (Initial Climb) | 817.10 | 14.61 | -53.71 | -194.79 | -111.35 |
| Climb | 855.58 | 8.16 | 18.01 | -57.24 | -12.73 |
| Cruise | 518.91 | 5.47 | 9.38 | -73.79 | -24.60 |
| descent | 124.04 | 0.30 | 79.21 | 60.13 | 71.41 |
| Landing | 72.25 | 0.12 | 85.72 | 72.62 | 80.37 |

It is observed from Table 9 that power error is $\pm 20\%$ with a wingspan (3.57) scaling factor for the climb and cruise phase of flight. Similarly, it is observed from Table 12 that the rate of energy consumption error is also $\pm 20\%$ with a wingspan (3.57) scaling factor for the climb and cruise phase of flight.

It is observed from Table 9 that the power error is $\pm 25\%$ with a MTOW (3.9) scaling factor for the climb and cruise phase of flight. Similarly, it is observed from Table 12 that the rate of energy consumption error is also $\pm 25\%$, with a MTOW (3.9) scaling factor for the climb and cruise phase of flight.

The energy consumption error in Table 10 using wingspan and MTOW as scaling factor for take-off, climb, descent, and landing phase is underestimated. The energy consumption scaled-up using the wingspan as the scaling factor for the cruise phase has the least amount of error, $\pm 31\%$. This was expected as the power required calculated for the cruise phase in Table 6 had $\pm 31\%$ error. The scaled-up energy consumption using wing loading and MTOW has a high percentage of errors in all flight phases.

With wing loading as a scaling factor, the power error and rate of energy consumption errors are much higher in all phases of flight. Hence it is not a suitable scaling parameter for scaling Albatross data. During the take-off and landing phases, data showed a high percentage of error for all three scaling factors.

All three scaling factors overestimated the power and rate of energy consumption in the take-off phase and underestimated it in the flight's descent phase (see Table 9, Table 12). The maximum power to weight ratio of Albatross is 0.15 kWh/kg, and the maximum power to weight ratio of Velis Electro is 0.10 kWh/kg. The maximum power to weight ratio of Albatross is higher than that of Velis Electro. At take-off, the Albatross lifts much

faster and with maximum thrust. Albatross takes off in minimum time and with maximum thrust. The power draw from batteries is maximum at take-off for Albatross. Hence it is overestimating the power and the rate of energy consumption during take-off.

The glide ratio of Velis Electro is 15:1, and the glide ratio of Albatross is 30:1. The power required is inversely proportional to the L/D ratio for a level flight. Albatross has a better performance cruise segment than Velis Electro.

The model was expected to fly at a scaled speed derived from Froude's number in Equation 14. In Table 13, the expected speed for the Albatross flight test is calculated from the Velis Electro using the scaling factors. The Albatross had an IAS, which was less than the scaled speed for the climb, cruise, and descent phases of flight. This lower speed affected the Reynolds number scaling estimates of the Albatross and Velis Electro. The Reynolds number of the Albatross test flight was less than the expected scaled value calculated from the Velis Electro speed profile. Albatross and Velis Electro flight tests were conducted on their respective optimal airspeed they were designed for rather than the scaled velocity.

Table 13 Speed scaling

| Unit - Knots | Climb Speed | Cruise Speed | Descent Speed |
|-------------------------|--------------------|---------------------|----------------------|
| Expected Speed (N=3.57) | 40 | 47 | 41 |
| Expected Speed (N=4.3) | 38 | 45 | 40 |
| Expected Speed (N=3.9) | 36 | 43 | 38 |
| Albatross IAS | 35 | 37 | 32 |

The Albatross underestimated the power, energy, and rate of energy consumption for the descent phase concerning all the scaling factors. Albatross has an L/D ratio almost double of Velis Electro. During the descent phase, the Albatross shut the engine down and glided for the landing at the earliest. The power, energy, and rate of energy consumption of Velis

Electro were almost the same as the cruise phase even after few minutes into the descent phase Figure 6. In Velis Electro, the power draw also increases right before the landing. The full-scale airplane is also designed for regenerative power in the descent phase of the flight.

The entire power train of Velis Electro is liquid-cooled for maintaining the optimal temperature range for the entire electronics operation. The model airplane does not have any cooling system installed.

The rate of climb to reach approximately 35 feet in Velis Electro (see Appendix B, Table 15) was 152 feet/min., the same for Albatross (see Appendix B, Table 14) was 618 feet/min. The rate of climb for the Albatross is higher, way higher than that of Velis Electro. A higher climb rate is one more reason for the overestimation of the power and rate of energy consumption by Albatross in the take-off phase.

The rate of climb of Albatross and Velis Electro in the climb phase was 185 feet/min., 174 feet/minute, respectively (See Appendix A, Table 14, Table 15). The difference in the rate of climb in the climb phase is not too high between Albatross and Velis Electro. The rate of descent of Albatross and Velis Electro were 366 ft./min, 132 ft./min, respectively (See Appendix A, Table 14, Table 15). As the Albatross descent at a much higher rate than Velis Electro and Albatross underestimate the energy consumption during this phase. During the climb phase, the airplane consumes more energy to gain kinetic and potential energy; the reverse happens at the descent phase. The airplane consumes less energy as it loses altitude, and potential energy changes into kinetic energy.

Albatross is a V-tail, two-blade pusher propeller with a small fuselage, while the Velis Electro is a T-tail, three-blade puller prop with a bigger fuselage.

The following equation calculates battery mass fraction [17]:

$$\mathbf{BMF} = \frac{m_b}{MTOW} \qquad \mathbf{Equation\ 28}$$

In the above equation m_b is the mass of the battery, MTOW is the maximum take-off weight. The model has a BMF of 0.13, and the full-scale airplane has a BMF of 0.24.

Chapter 5

Conclusion

This study aimed to understand the possibility and develop scaling laws to estimate the power and energy consumed by a full-scale airplane using a subscale model. This study concludes that a scaling factor used for developing a geometrical subscale model can also be used to estimate the power and rate of energy consumption. The power required in a level flight is directly proportional to wingspan, wing loading, and MTOW. Hence any of these parameters can be used as a scaling factor. The model airplane used in this study was not a geometrically perfect subscale model. All three scaling factors were used to validate the theory.

The power required results captured in Table 6 shows that in a model with ideal dimensions, it is possible to use the wingspan, Wing Loading or MTOW as the scaling factors. Table 6 also shows that this study's model will have inherent errors in the range of $\pm 35\%$ based on which parameter is used for scaling.

Power errors and the rate of energy consumption errors were found to be in the range of $\pm 20\%$ for climb and cruise flight phases, with the wingspan as the scaling factor. Using the MTOW as the scaling factor, the estimates of power errors and rate of energy consumption errors were in the range of $\pm 30\%$ in the climb and cruise phase of flight.

The error in energy consumption using the wingspan as the scaling factor was $\pm 30\%$ in the cruise phase. The energy estimates in other phases of flight were either overestimated or underestimated using all three scaling factors. Wing Loading was not a good scaling factor, resulting in a much higher error for all the flight phases.

Chapter 6

Recommendations

The scaling laws developed in this thesis were validated using the flight data available from one test flight data of Velis Electro and one set of flight test data available from Albatross. The scaling factor calculated by wingspan and wing loading worked for this set of data. The theory can be validated by having multiple flight test data from Velis Electro and Albatross.

The theory is validated by using Albatross and Velis Electro, which are two geometrically different airplanes. Albatross is a V-tail, two-blade pusher propeller, while the Velis Electro is a T-tail, three-blade puller prop. Theoretically, puller propeller airplanes have a better performance in terms of rate of climb. The pusher propeller performance is affected by the separated boundary layer by the fuselage body. The Albatross has a two-blade propeller, while Velis Electro had a three-blade propeller. Furthermore, the diameter of the Albatross propeller is less than the scaled value from Velis Electro. To generate more thrust, the Albatross has to rotate at higher RPM; it consumes more power from batteries.

The test data from multiple geometrically scaled airplanes and full-scale airplanes with a scaled flight plan trajectory and scaled velocity profile shall be compared to get a better validation.

References

- [1] J. R. Chambers, "Modelling Flight: The role of dynamically scaled free-flight models in support of NASA's aerospace programs," National Aeronautics and Space Administration, Washington, D.C., 2010.
- [2] Electronic Code of Federal Regulations, Title 14, Chapter I, Subchapter C, Part 23, Subpart B, §23.1337.
- [3] M. Hepperle, "Electric Flight - Potential and Limitations," in *AVT-209 Workshop on ENERGY EFFICIENT TECHNOLOGIES AND CONCEPTS OPERATION*, 2012.
- [4] A. S. R. H. E. P. a. S. W. M. Duffy, "Propulsion Scaling Methods in the Era of Electric Flight," in *AIAA/IEEE Electric Aircraft Technologies Symposium (EATS)*, Cincinnati, OH, 2018.
- [5] P. & G. C. & P. C. & I. A. & H. M. Vratny, "Battery Pack Modeling Methods for Universally-Electric Aircraft," in *4th CEAS Air & Space*, Linköping, Sweden, 2013.
- [6] D. H. a. J. C. Sydney L. Schnulo, "Further Development and Validation of NASA X-57 Maxwell Mission Planning Tool for Mods III and IV," *Aerospace Research Central*, no. AIAA 2019-4491, 2019.
- [7] "Velis Electro," Pipistrel, [Online]. Available: <https://www.pipistrel-aircraft.com/aircraft/electric-flight/velis-electro-easa-tc/>. [Accessed 26 02 2021].
- [8] Paul Bertorelli, "AVweb," AVweb, [Online]. Available: <https://rb.gy/hsjd6d>. [Accessed 31 10 2020].
- [9] Applied Aeronautics, "Lithium Ion Batteries," Applied Aeronautics, [Online]. Available: <http://store.appliaeronautics.com/lithium-ion-batteries/>. [Accessed 31 10 2020].

- [10] Dossier, "E-Mobility Engineering Magazine," [Online]. Available: <https://www.emobility-engineering.com/post/dossier-pipistrel-alpha-electro>. [Accessed 01 02 2021].
- [11] J. S. B. J. W. P. G. Chester H. Wolowicz, "Similitude Requirements and Scaling Relationships as Applied to Model Testing," NASA Technical Paper, 1979.
- [12] S. S. G. K. A. Pesaran, "Temperature Extremes on Large Format Li-Ion Batteries for Vehicle Applications," in *30th International Battery Seminar*, Ft. Lauderdale, Florida, 2013.
- [13] V. S. N. U. S. K. S. S. P. C. A. L. J. S. K. S. Kamonpan Chumpolrat, "Effect of Ambient Temperature on Performance of Grid-Connected Inverter Installed in Thailand," *International Journal of Photoenergy*, vol. 2014, no. Article ID 502628, 2014.
- [14] E. C. o. F. Regulations, "Title 14, Chapter I, Subchapter F, Part 107, Subpart B, §107.51 "Operating limitations for small unmanned aircraft"."
- [15] "PX4 Flight Review," Pixhawk, [Online]. Available: <https://logs.px4.io/>. [Accessed 14 2 2021].
- [16] "Flight log Analysis," Pixhawk, [Online]. Available: https://docs.px4.io/v1.11/en/log/flight_log_analysis.html. [Accessed 14 02 2021].
- [17] D. P. Raymer, "Electric Propulsion," in *Aircraft Design: A conceptual Approach 6th Edition*, American Institute of Aeronautics and Astronautics, Inc, 2018.

Appendix A

Flight Data Analysis Tables

Table 14 Albatross Flight test trajectory

| Phase of flight | Phase duration | Avg Indicated Airspeed (Knots) | Avg. Temp | Avg. voltage | Avg. Current | discharged_mah | Energy Consumed (Wh) | Battery Discharge (%) | Change in altitude | Rate of change in altitude (feet/min.) | Power Albatross (kW) |
|----------------------------|-----------------------|---------------------------------------|------------------|---------------------|---------------------|-----------------------|-----------------------------|------------------------------|---------------------------|---|-----------------------------|
| Takeoff (Ground roll) | 0.09 | 10.12 | 25 | 25 | 34 | 54 | 1.3 | 0 | 5 | 0 | 0.85 |
| Takeoff (Initial Climb) | 0.06 | 27.52 | 25 | 23 | 45 | 37 | 0.9 | 0 | 37 | 619 | 1.05 |
| Climb | 0.56 | 37.59 | 25 | 25 | 20 | 182 | 4.6 | 1 | 104 | 184 | 0.50 |
| Cruise | 6.69 | 36.88 | 24 | 25 | 13 | 1442 | 36.6 | 10 | -49 | -7 | 0.33 |
| descent | 0.27 | 27.31 | 23 | 26 | 0 | 3 | 0.1 | 0 | -99 | -367 | 0.01 |
| Landing | 0.16 | 19.66 | 23 | 26 | 0 | 1 | 0.0 | 0 | -4 | -24 | 0.01 |

Table 15 Velis Electro Flight Test Data

| Phase of Flight | Phase duration | Avg. bat 1 Current | Avg. bat 1 Voltage | Avg. bat 2 Current | Avg. bat 2 voltage | Used Capacity 1 (SOC) | Used Capacity 2 (SOC) |
|--------------------------|---------------------------|----------------------------|----------------------------|---------------------------------|---------------------------|------------------------------|------------------------------|
| Take off (Ground Roll) | 0.81 | 49.89 | 376.78 | 49.52 | 376.17 | 0.00 | 0.00 |
| Take off (Initial Climb) | 0.24 | 67.53 | 367.25 | 66.05 | 366.81 | 1.00 | 1.00 |
| Climb | 3.36 | 71.97 | 360.46 | 70.53 | 360.03 | 14.00 | 13.00 |
| Cruise | 6.15 | 43.30 | 360.66 | 43.08 | 360.15 | 16.00 | 15.00 |
| Descent | 4.00 | 10.06 | 367.77 | 10.19 | 367.21 | 3.00 | 3.00 |
| Landing | 1.00 | 5.85 | 370.21 | 5.87 | 369.57 | 0.00 | 1.00 |
| Phase of Flight | Power of Battery 1 | Bat 1 avg cell temp | Bat 2 avg cell temp | Average Requested Torque | Motor RPM | Avg. motor power | Avg. motor temp |
| Take off (Ground Roll) | 18796 | 26 | 26 | 942 | 2249 | 36 | 42 |
| Take off (Initial Climb) | 24798 | 26 | 27 | 791 | 2211 | 49 | 51 |
| Climb | 25941 | 29 | 29 | 800 | 2324 | 51 | 64 |
| Cruise | 15618 | 32 | 32 | 511 | 2215 | 31 | 64 |
| Descent | 3701 | 32 | 32 | 127 | 1605 | 7 | 55 |
| Landing | 2167 | 31 | 31 | 101 | 852 | 4 | 50 |

| Phase of Flight | IAS (Knots) | Avg. inverter temp | Avg. bat 1 cooling temp | Avg. inverter cooling temp 1 | Avg. inverter cooling temp 2 | Remaining flight time | Pressure Altitude Change |
|--------------------------|------------------------|--|--|--|--|------------------------------|---|
| Take off (Ground Roll) | 15 | 36 | 27 | 34 | 33 | 20 | 0 |
| Take off (Initial Climb) | 64 | 45 | 28 | 41 | 43 | 19 | 36 |
| Climb | 75 | 48 | 29 | 43 | 48 | 19 | 586 |
| Cruise | 89 | 43 | 31 | 40 | 44 | 25 | -100 |
| Descent | 79 | 38 | 31 | 37 | 39 | 38 | -528 |
| Landing | 35 | 39 | 32 | 39 | 39 | 37 | 4 |
| Phase of Flight | Power Battery 2 | Total Power from Battery 1 & 2 (kW) | Energy Consumption (using avg. motor power) | Energy Consumption (bat. 1) (kWh) | Energy Consumption (bat. 2) (kWh) | Total Energy (kWh) | Rate of change in altitude (feet/min.) |
| Take off (Ground Roll) | 18628 | 37.42 | 0.49 | 0.26 | 0.25 | 0.51 | 0 |
| Take off (Initial Climb) | 24228 | 49.03 | 0.19 | 0.10 | 0.10 | 0.19 | 152 |
| Climb | 25394 | 51.33 | 2.85 | 1.45 | 1.42 | 2.88 | 174 |
| Cruise | 15516 | 31.13 | 3.14 | 1.60 | 1.59 | 3.19 | -16 |
| Descent | 3742 | 7.44 | 0.45 | 0.25 | 0.25 | 0.50 | -132 |
| Landing | 2168 | 4.33 | 0.06 | 0.04 | 0.04 | 0.07 | 4 |

Appendix B

Flight Data Analysis Plots

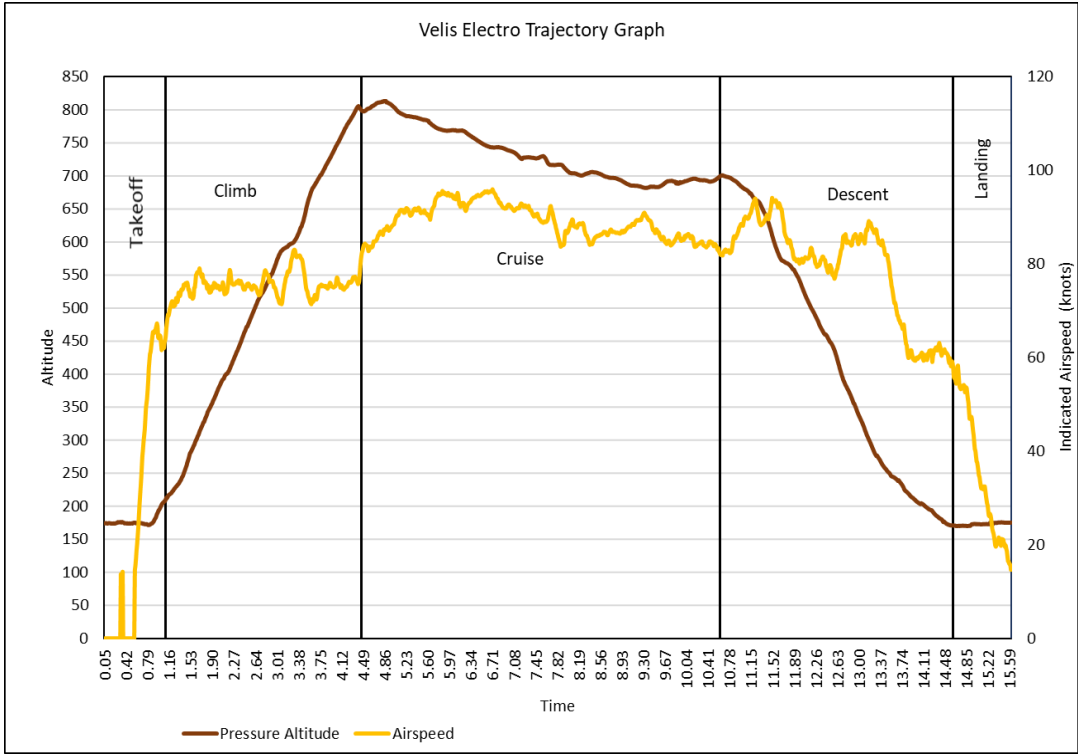


Figure 8 Velis Electro Altitude and Airspeed graph

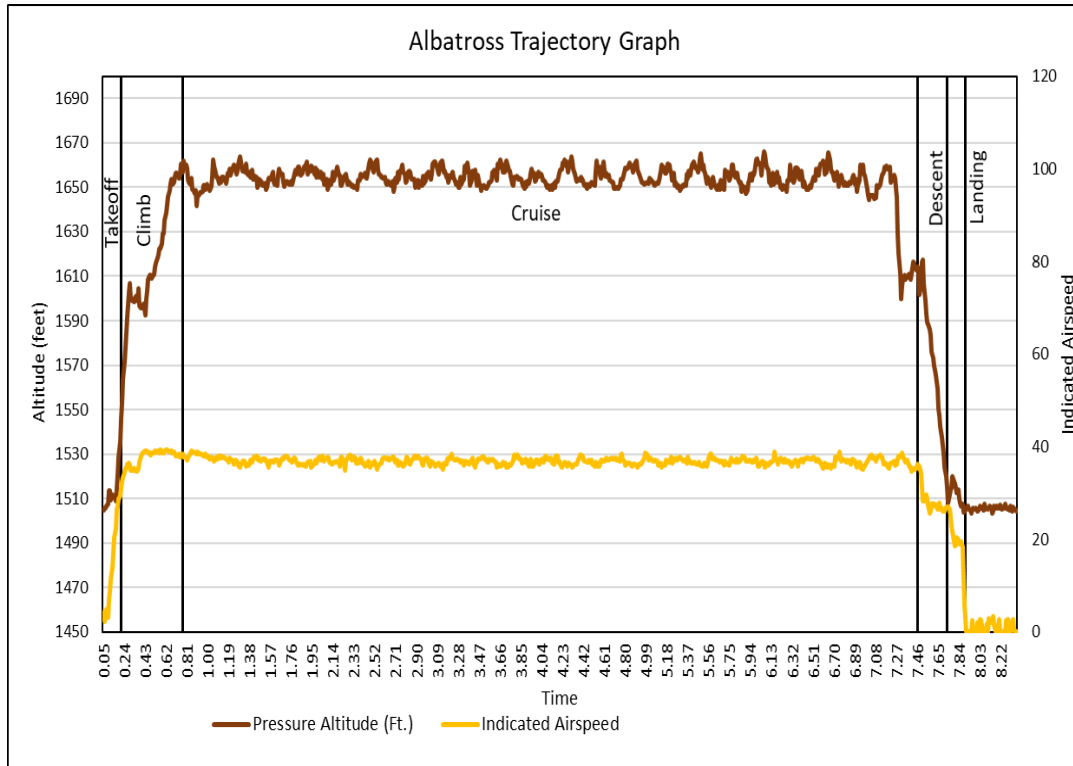


Figure 9 Albatross Altitude and Airspeed graph